Q-Band Single-Layer Planar Fabry-Pérot Cavity Antenna with Single Integrated-Feed

Seyed A. Hosseini[*], Filippo Capolino, and Franco De Flaviis

Abstract—An extremely simple design of a planar Fabry-Pérot cavity antenna is proposed as a very promising candidate for millimeter-wave wireless systems. The simplicity of this design is obtained by using a dielectric slab, here quartz, to form a *single-layer* cavity with thin layers of copper etched/printed on both sides, to form the ground plane on one side and the frequency-selective surface (FSS) on the opposite side of the slab. By keeping the planarity of the structure and not-requiring an additional supporting layer, the cavity is excited using an integrated feeding-slot antenna etched on its ground plane. The variations in the radiation properties of the proposed antenna, linked to its leaky-wave behavioral explanation, are studied by designing three prototypes with different maximum gain values. The prototype FPCs are designed to operate for Q-band wireless communication systems (here, resonating at three different frequencies in the range of 42–46 GHz). The performance of the designed antennas, backed by initial analytical and numerical simulations, is verified with a full set of measurement results.

1. INTRODUCTION

Three different factors play important roles in popularity of an antenna to be used for majority of wireless millimeter-wave (MMW) applications (e.g., Q-band inter-satellite wireless communication systems [1]); the highly-efficient directive radiation for compensating losses associated with structural and wireless-path losses, planarity of antenna structure aiming for smaller spatial spacing being used by the antenna, and finally, the planarity and integrability of the antenna-feed aiming for simplicity of integration with other part of the system. As an example, planar array antennas are well-known for their ability to produce high-gain directive radiation at MMWs, as shown in [2, 3]. However, considering the fact that each element of the array must be excited separately, the main drawback of such antennas can be related to the losses associated to their complex feeding network. On the other hand, planar Fabry-Pérot cavity (FPC) antennas are known for their ability to produce highly-efficient directive radiation only using a single feeding point [4, 5]. Planar FPCs can be formed by placing a partially-reflective surface (PRS) on top of a ground plane, as well described in [4, 5]. The radiation behavior of these antennas rely on the excitation of leaky-waves (LW) inside the cavity [5]. However, one of the main constraints of such cavities is their 3 dB power/gain bandwidth as discussed in [6, 7].

MMW FPC antennas have been studied using various fabrication and feeding techniques backing the fact that these cavities are one of promising solutions to produce highly-efficient directive radiation at such high frequencies. To the extent of our knowledge, there is only a handful of FPC antenna designs being fabricated and measured at MMW frequencies (i.e., operating at frequencies higher than 30 GHz) as in [8–11]; among all of them, it can be seen that their structures consist of a multi-layer cavity and/or a multi-layer configuration to support the feeding antenna. Moreover, some of the designed antennas are fed using a non-planar feed (e.g., a waveguide opening in the ground plane as in [8, 10]).

More recently, in some very brief presentations [12, 13], two novel designs of single-layer dielectric-based cavities excited using integrated slot antenna on their ground plane, and operating at around 44 GHz and 60 GHz, respectively, were presented. In those works, without providing a complete analysis behind the designs, only few selected measurement plots were shown. Being able to print/etch the frequency-selective surface (FSS) and integrated antenna (without requiring any additional layer and compromising the planarity of the structure) on top/bottom surfaces of the slab (i.e., the cavity) is one of the very interesting aspects of this design.

In this work, following the brief introductory presentations in [12, 13], a comprehensive study on the design and radiation performance of FPCs made of a simple single-layer structure, will be proposed. In order to show the feasibility of this design at MMWs, and also to study the variations in the radiation features of such cavity, three prototype antennas with different maximum gain values are designed and fabricated. Here, some new discussions (compared to what was briefly discussed in [12, 13]) will be made which will be very helpful to understand the radiation performance of this type of antenna. These discussion can be listed as follows. First, using some analytical calculations, based on the frequency-dependent model of the each FSS layer and the transmission-line (TL) model of the antenna, the accepted gain and the gain bandwidth of the designed antennas are estimated which later will be compared to the full-wave and measurement results. Second, by linking the radiation performance of each cavity to the dominant LWs excited inside the cavity, some interesting aspects of these antennas will be highlighted which will provide the reader with a better understanding of the full-wave and measurement results. Third, after introducing the integrated-slot, designed to excite each cavity, it will be shown that the feeding-slot has no impact on the directivity of the FPCs and it is only designed to launch the LWs inside the cavity. Forth, a full set of measurement results are presented for all the three cases analyzed here, and it will be compared to the values obtained from both analytical and full-wave simulation results. In these results, besides showing the measured reflection coefficient and broadside radiation gain of the antenna, E-plane and H-plane radiation patterns, will be shown at the central operating frequency as well as two other frequencies in the operative bandwidth. Finally, looking at the measurement results, some important observations will be listed which can be useful in future designs of such cavities.

2. THE THEORETICAL DESIGN OF THE ANTENNAS

Figure 1(a) shows layered view of the proposed antennas. The cavity is made of a quartz substrate covered by a very thin metallic FSS on the radiating side and a ground plane on the other side. The cavity is fed by an integrated slot-dipole (i.e., magnetic current) printed on its ground plane as it will be discussed.
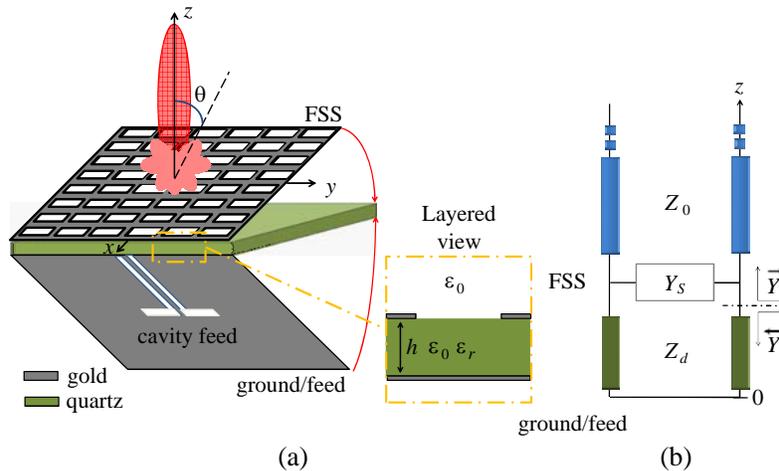
Figure 1. (a) Layered view of the proposed FPC antenna. (b) TL model for a FPC antenna formed by a very thin FSS.

Using reciprocity theorem and the TL model of a FPC antenna, as discussed in [14] and shown in Figure 1(b), the radiation performance of the antenna can be found as a function of the design parameters, i.e., relative permittivity of the dielectric filling the cavity and the reflectivity of the FSS. In the TL model of the antenna, the free space above the FPC antenna has a characteristic wave impedance $Z_0 = Y_0^{-1} = \sqrt{\mu_0/\varepsilon_0}$, whereas the cavity with height h represents the dielectric slab with the characteristic impedance $Z_d = Y_d^{-1} = Z_0/\sqrt{\varepsilon_r}$ where ε_r is the relative permittivity of the material inside the cavity. Furthermore, in the TL model of the antenna it is assumed that FSS and the cavity are extended infinitely along the xy-plane, and the FSS has a thickness much smaller than the wavelength, and thus it is modeled as a shunt admittance $Y_S = jY_0\hat{b}$, where $\hat{b}$ is its normalized susceptance [4–7]. Note, $\hat{b}$ is in general negative for an inductive FSS (i.e., periodic slots) and is positive for a capacitive FSS (i.e., periodic patches) [4–7]. The upward and downward admittances just below the interface of FSS and cavity, as shown in Figure 1(b), are $\overrightarrow{Y} = Y_0 + Y_S$ and $\overleftarrow{Y} = -jY_d \cot(kh)$ respectively, where $k = k_0\sqrt{\varepsilon_r}$ and $k_0 = \omega\sqrt{\mu_0\varepsilon_0}$. The total imaginary admittance calculated just below the FSS is $B_{tot} = \text{Im}(\overrightarrow{Y} + \overleftarrow{Y})$ which vanishes at the resonance frequency of the cavity f_{res}, leading to the expression of the resonance height of the cavity

$$h = \frac{1}{k_{res}} \cot^{-1}\left(\frac{Y_S}{j\sqrt{\varepsilon_r}Y_0}\right) = \frac{1}{k_{res}} \cot^{-1}\left(\frac{\hat{b}}{\sqrt{\varepsilon_r}}\right), \tag{1}$$

where $k_{res} = 2 * \pi * f_{res} * \sqrt{\mu_0 * \varepsilon_0 * \varepsilon_r}$, as in [4–7]. The permittivity of quartz substrate (produced by [15] with the nominal thickness of 1.5875 mm) is equal to 4 with a very low dielectric loss tangent below 0.001 at the desired frequency band. A very thin layer of gold (i.e., 5 μm) was deposited on both sides of the quartz substrate as a conducting sheet. Linear-polarized FPCs formed by thin metallic FSSs made of periodic rectangular slots have been designed. The slot dimensions for each FSS, as shown in Figure 2(a), have been selected to achieve different FSS reflectivity values, and hence different antenna gain (i.e., low-gain (LG), medium-gain (MG) and high-gain (HG) FPC antennas). All FSS unit-cells are square with side $U = 1.8$ mm, corresponding to less than half wave-length at the designed frequency of the FPC. The value of $\hat{b}$ versus frequency for each FSS, as shown in Figure 2(b), can be found by using numerical simulations of the FSS alone with a quartz dielectric below and air above, by imposing periodic boundaries.

The frequency-dependent susceptance of the FSSs, shown in Figure 2(b), is used to evaluate the gain plots shown in Figure 2(c) calculated by using the formula discussed in [16], based on the spectral representation of the dipolar field and a TL model. In theoretical TL calculations in Figure 2(c), gain denotes the "accepted gain" G_A of the antenna fed by an ideal magnetic current (i.e., a slot) on the ground plane of the cavity. It is defined as the radiated power density over the input (and not the incident) power averaged over the whole solid angle. Moreover, G_A accounts for the power lost in
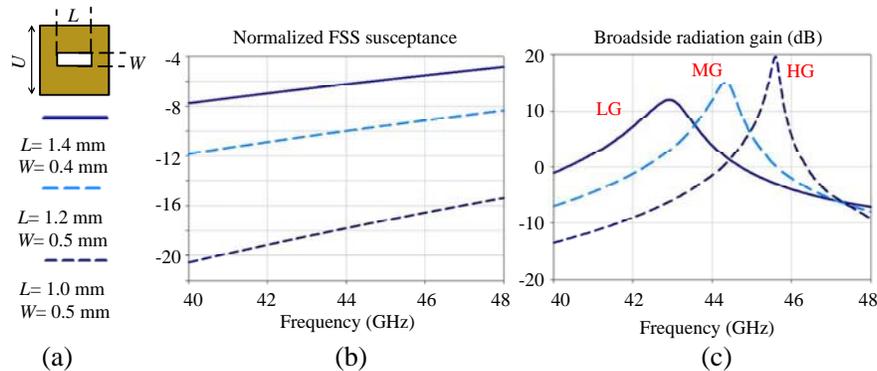
Figure 2. (a) The designed FSS unit-cells. (b) Normalized susceptance $\hat{b}$ modeling the FSS versus frequency. (c) The broadside accepted gain of the designed FPC antennas versus frequency (using formulas in [16]).

Table 1. Designed features of the FPC antennas.

FPC	$\hat{b}$	f_{res} (GHz)	f_G (GHz)	Gain (dB)	GBW (GHz)
Low Gain (LG)	-6.6	43.03	42.9	12	1.11
Medium Gain (MG)	-9.8	44.43	44.35	15.15	0.58
High Gain (HG)	-16.6	45.68	45.6	19.6	0.21

possible planar cavity modes (i.e., the surface-waves excited in the quartz dielectric slab), other than the one used for leaky-wave radiation. Moreover, as shown in Figure 1, the feeding slot radiates both backward to air and forward into the FPC and then to air through the FSS. Consequently, in the gain calculations (using the TL model of antenna and the formulas proposed in [16]), the total radiated power is defined as a sum of total forward and backward radiated power from the feeding slot (i.e., ideally a magnetic current). Since all the FPC antennas are fabricated on the same quartz disk with a fix thickness $h = 1.5875$ mm, the antennas, based on (1), resonate at slightly different frequencies. Table 1 shows the maximum radiation gain, the frequency f_G at which it occurs, and 3 dB gain BW (GBW, defined as the frequency range where the broadside gain remains within the -3 dB-level of its maximum value) for the designed FPC antennas.

In Table 1, it is shown that frequency f_G is slightly different from "resonance" frequency of the cavity, f_{res}, and that the two tend to coincide for higher gains. Also, note that the higher the gain is, the narrower the bandwidth is, according to what described in [4–7]. Table 1 shows that the gain is directly proportional to $|\hat{b}|$ (evaluated at f_{res}), in agreement with [4–7].

3. LEAKY-WAVES EXPLANATION FOR FPC ANTENNAS

In order to provide a better physical insight into the radiation performance of the designed antennas, the propagation and attenuation constants, β and α, of the TE and TM LWs excited in the FPC are studied here. A detailed explanation on the analytical calculations can be found in [5], and the authors, for the sake of brevity, would like to refer the readers to [5] for all related details. The dispersion relation of the LW transverse wavenumber $k_t = \beta - j\alpha$ (i.e., either along x or y as shown in Figure 1) of dominant TE and TM leaky-waves excited in the FPC, versus frequency, can be found based on equations in [5]. The dispersion diagram (the plot of β and α versus frequency) of the TE and TM LWs, for each cavity, is shown in Figures 3(a) to (c). Notably, the frequency variations of the reflectivity of the FSS layer ($\hat{b}$ versus frequency), shown in Figure 2(b), is considered in the calculations.

Looking at Figures 3(a)–(c), the main observations can be listed as follows:

1) At proximity of f_G of each cavity, the LW attenuation and propagation constants holds the same value for both TE and TM waves satisfying the optimum condition as discussed in [5].
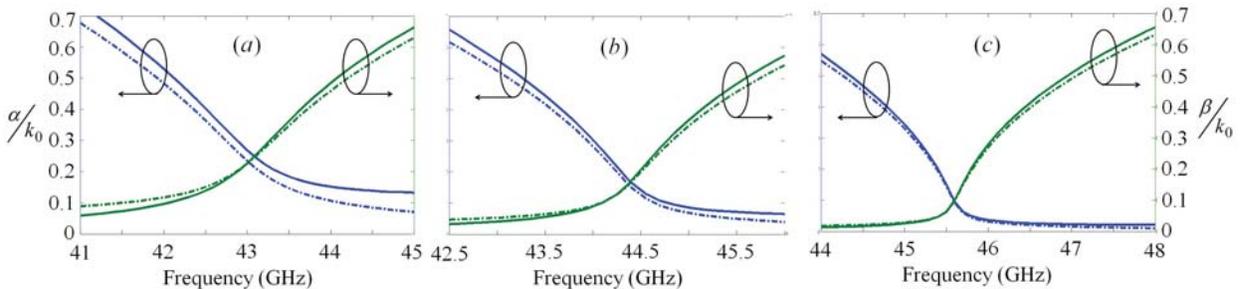
Figure 3. The LW dispersion diagram for, (a) the LG FPC antenna, (b) the MG FPC antenna, and (c) the HG FPC antenna. Note, in these plots solid and dashed lines are for TM and TE waves, respectively.

2) The frequency of the optimum condition, converges to a single frequency for both TE and TM waves, as the gain of the antenna increases (i.e., more reflectivity for the FSS or larger absolute value for $\hat{b}$). Moreover, for high-gain FPC antennas, the optimum frequency coincides with the resonance frequency of the cavity.

3) The magnitude of α/k_0 holds a very small value for high-gain FPC antennas corresponding to less amount of leakage/loss per unit-distance, thus larger effective radiation area for the antenna (i.e., more radiation gain).

4) Looking at the left side of the optimum frequency (i.e., lower frequencies), β/k_0 remains very small while α/k_0 increases. The small value of β/k_0, corresponds to almost a uni-phase radiation from the cavity equivalent to a broadside beam. However, since α/k_0 is larger than its value at the optimum frequency, the antenna has a smaller radiation gain [4, 5] with respect to its maximum value.

5) Looking at the right side of the optimum frequency (i.e., higher frequencies), α/k_0 remains very small while β/k_0 increases. Smaller α/k_0 equivalents to less leakage/loss per unit-distance thus higher effective radiation area (i.e., more radiation gain). However, since β/k_0 increase, the antenna loses its uni-phase aperture resulting in a cone-shape beam (i.e., opening from the middle) as discussed in [4, 5]. This point and the previous one will be verified later based on measurement results.

4. FEEDING OF A SINGLE-LAYER FPC ANTENNA

FPC antennas can be excited with either an external feeding structure such as a coaxial cable (e.g., inserted through a hole into the ground plane of the cavity, forming a dipole inside the cavity [17]) or a waveguide opening [8, 10, 18], or patch antennas as in [16]. Here, instead, by using a planar feed on the ground plane of the cavity, we are showing that this single-layer FPC antenna is a promising candidate for planar low-cost MMW technology (decreasing number of layers is a key factor in reducing the complexity of the structure, related structural losses, and the fabrication cost, especially at MMWs).

Figure 4(a) shows the three sections of the proposed feeding structure. The first section is a gap of $g_1 = 300\,\mu\text{m}$ chosen before the starting point of the CPW line, in a way to avoid additional loading to the probe-landing point which can change the reflection coefficient of the antenna. The second section of the feed is a CPW with characteristic impedance of 60 Ohm. This value remains practically constant over the desired frequency band of 42–46 GHz. Our fabrication constraints and ease of probing was the reason to feed the antenna with 60 Ohm line instead of typical 50 Ohm line. The CPW line, shown in Figure 4(a), is designed with the gap size of $g_2 = 50\,\mu\text{m}$ and the line-width of $W_{\text{CPW}} = 200\,\mu\text{m}$. For
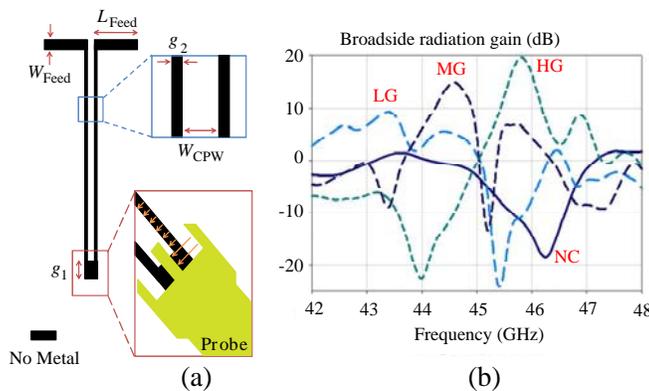
Figure 4. (a) Each FPC antenna is fed by a coplanar-waveguide-fed slot-dipole on the ground plane (power is provided using the ground-signal-ground (GSG) probe at the other end of CPW). (b) Simulated broadside radiation gain of the proposed antennas versus frequency compared to same-size slab not covered (NC) by any FSS layer.

each antenna, the CPW feeds a slot-dipole placed at the center of the FPC ground plane. The length of the slot-dipole is optimized in order to resonate around the resonance frequency of the FPC antenna. Therefore, the slot length L_{Feed} is equal to 1.22 mm for the LG FPC antenna, and equal to 1.12 mm for all other antennas, whereas the width of the slot W_{Feed} is equal to 300 μm for all cases.

Figure 4(b) shows the broadside radiation gain of the designed antennas (full-wave simulations by Ansys HFSS, i.e., based on the finite element method) considering 20 by 20 element in each covering FSS. For completeness, we compare such gain with the case where there is no FSS covering the slab (NC). It can be seen that the in the NC case, the broadside radiation shows a gain of around or below 0 dB; therefore, it can be seen that the radiation gain of such FPCs are mainly function of cavity parameters than the feed. In other words, it is the presence of the cavity that is responsible for the antenna gain.

5. MEASURED AND FULL-WAVE SIMULATION RESULTS

In order to fabricate the designed antennas, the formulas discussed in [16] are used to select the number of FSS elements of each antenna (20 by 20 element) aiming at negligible LW field strength (i.e., below −25 dB relative to the maximum field strength at the center of each cavity) at the edges of each truncated antenna eliminating the unwanted edge diffraction effect. The fabrication of the designed antennas was done in our clean rooms in the Integrated Nanosystems Research Facility (INRF) at the UC Irvine using standard fabrication process. The top and bottom views of the antennas fabricated on the quartz disk are shown in Figures 5(a) and (b) respectively. The close-view of the FSS layer and the fabricated feeding line are shown in Figures 5(c) and (d), respectively. The numbers 1, 2 and 3 shown in Figures 5(a) and (b) are associated to LG, MG and HG FPC antennas, respectively. Figure 6(a) shows the measured and simulated reflection coefficient of the LG FPC antenna. There is a reasonable agreement between the results. Notably, the reflection coefficient shows a resonance at approximately 43.3 GHz which is very close to the theoretical design value based on TL theory (42.9 GHz) shown in Table 1. Figure 6(b) shows the measured and simulated normalized broadside realized gain, defined as $G_R = G_A(1 - |\Gamma|^2)$, of the FPC antenna versus frequency. The antenna has maximum gain at $f_G = 43.3$ GHz, very close to the impedance resonance frequency, where the antenna reflection coefficient is minimum. Figure 6(c) shows the simulated and measured normalized gain patterns of the antenna in both E and H-plane (xz-plane and yz-plane, respectively, as shown in Figure 1) at different frequencies around the measured f_G (43.3 GHz).
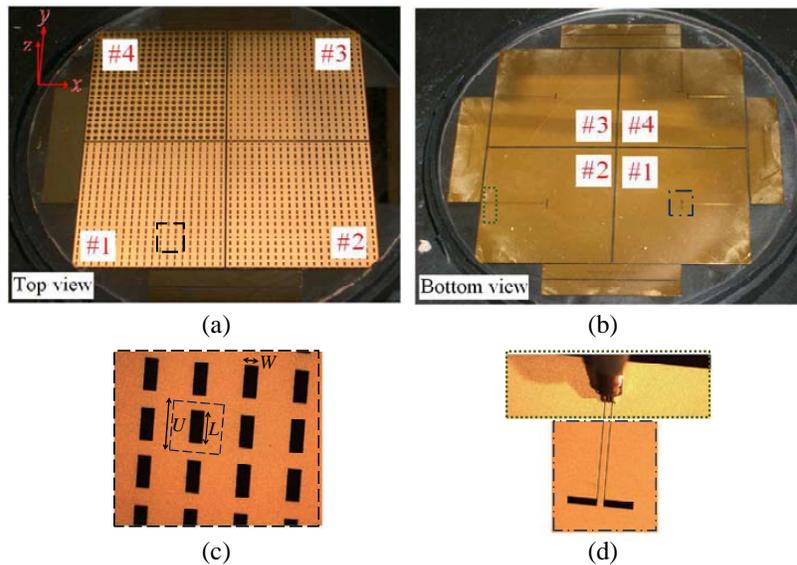
Figure 5. Top and bottom views of the fabricated antennas, (a) and (b), respectively. The close-ups of (c) the FSS, and of (d) the CPW line with probe used for measurements and the slot-dipole.
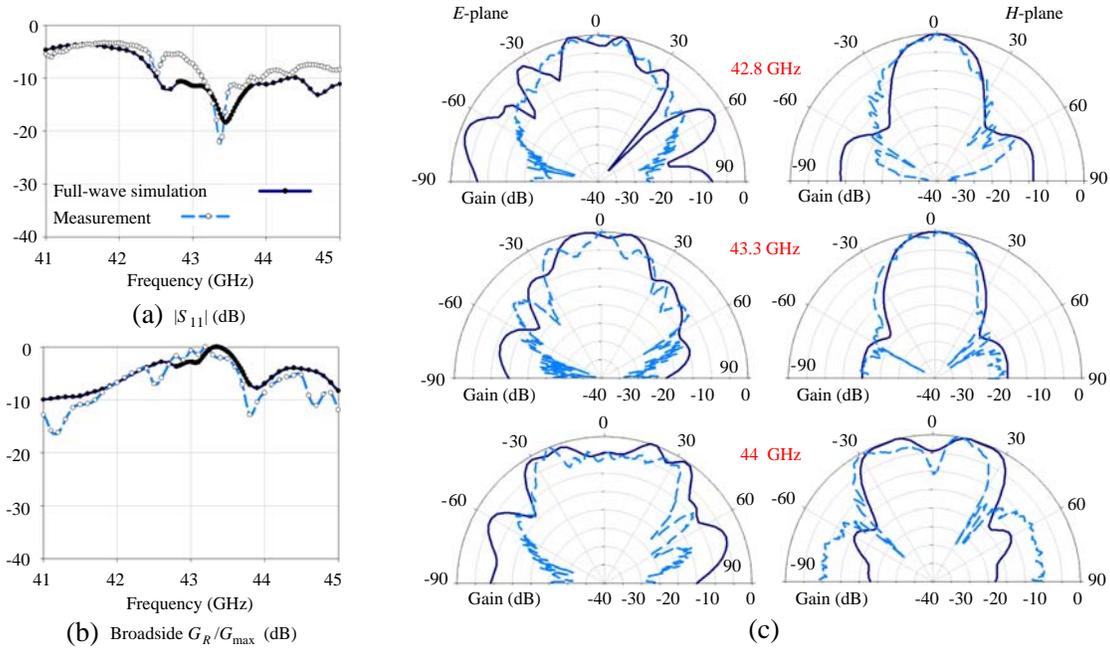
Figure 6. (a) The reflection coefficient, (b) the normalized realized broadside gain of the LG FPC antenna, (c) the normalized gain patterns in both E and H-planes (a comparison between the full-wave simulation and measurement results).

The antenna has a directive pattern at broadside around its resonance frequency; however, for higher frequencies, the pattern starts opening at broadside, in accordance with pattern behavior of planar LW antennas discussed in Section 3. Furthermore, it can be seen that the radiation pattern of the antenna, in the H-plane, is symmetric while the pattern in the E-plane is not. Moreover, It can be seen that in the E-plane, the simulated patterns are different from the measured ones. This can be explained due to the fact the feeding line of the antenna is located along the E-plane. Figure 7(a) shows the measured and simulated reflection coefficient of the MG FPC antenna versus frequency. There is a good agreement between the measured reflection coefficient of the antenna and the simulated one. Figure 7(b) shows the measured and simulated normalized realized broadside gain of the antenna versus frequency with a peak at $f_G = 44.6$ GHz. The theoretical (TL) value of f_G (44.35 GHz) is almost the same as both measured and simulated values at approximately 44.6 GHz. The normalized gain patterns of the antenna, in the both E and H-planes, at different frequencies around the measured f_G (44.6 GHz), are shown in Figure 7(c). Analogously to the low-gain case in Figure 6(c), the radiation patterns, in the E-plane of the antenna, are asymmetric. However, it can be seen that the impact of the feeding line was less than the low-gain antenna case.

Figure 8(a) illustrates the measured and simulated reflection coefficients of the HG FPC antenna. Although the measured reflection coefficient of this antenna tends to follow the general frequency behavior of the simulated results, the reflection coefficient levels are different. This can be explained due to a very important fact. The probe-landing distance to the center of the cavity is designed to be the same for all designed cavities (i.e., LG, MG and HG antennas). For the HG antenna, the effective radiation aperture of the antenna increases, and the field level of the LWs is stronger at a fixed distance than one of the lower-gain FPC antennas. Therefore, the loading of the probe-head (while feeding the antenna) has a larger impact on the measured reflection coefficient of the HG antenna than ones of the lower-gain antennas.

The measured and simulated normalized realized broadside gain of the antenna is shown in Figure 8(b). Figure 8(c) shows the normalized gain pattern of the antenna in both E and H-planes at frequencies around the measured f_G (45.8 GHz). It can be seen that the simulated and measured patterns are in a good agreement. There is slight asymmetry in the radiation pattern of the antenna in
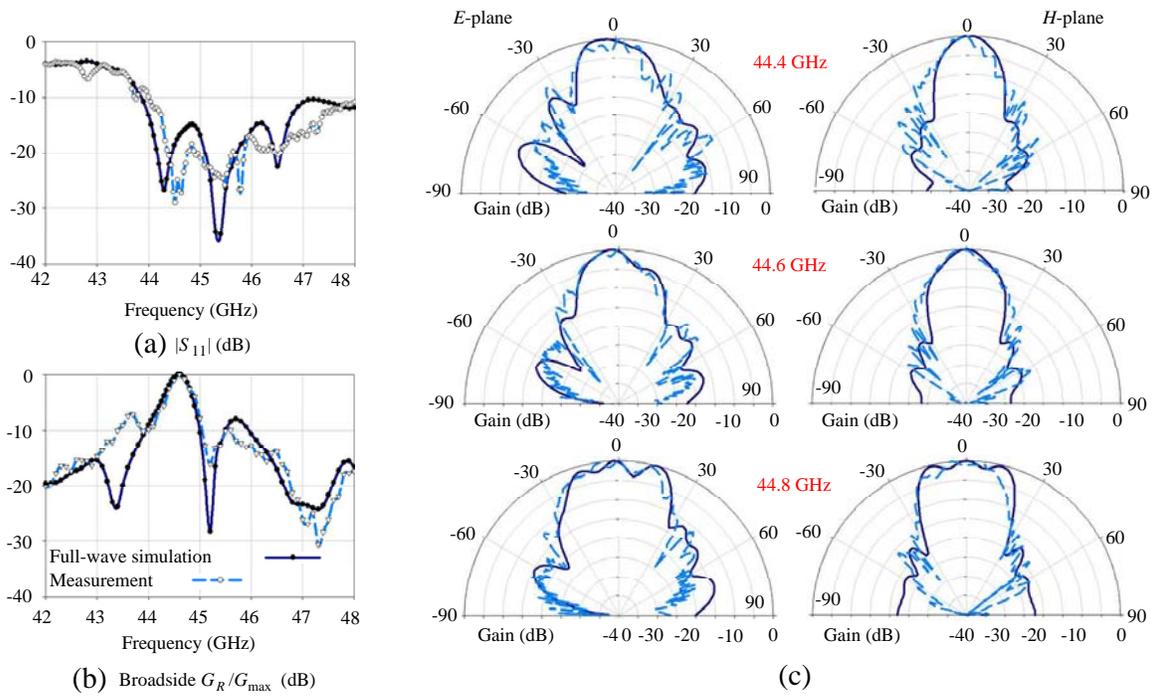
Figure 7. (a) The reflection coefficient, (b) the normalized realized broadside gain of the MG antenna, (c) the normalized gain patterns in both E and H-planes (a comparison between the full-wave simulation and measurement results).
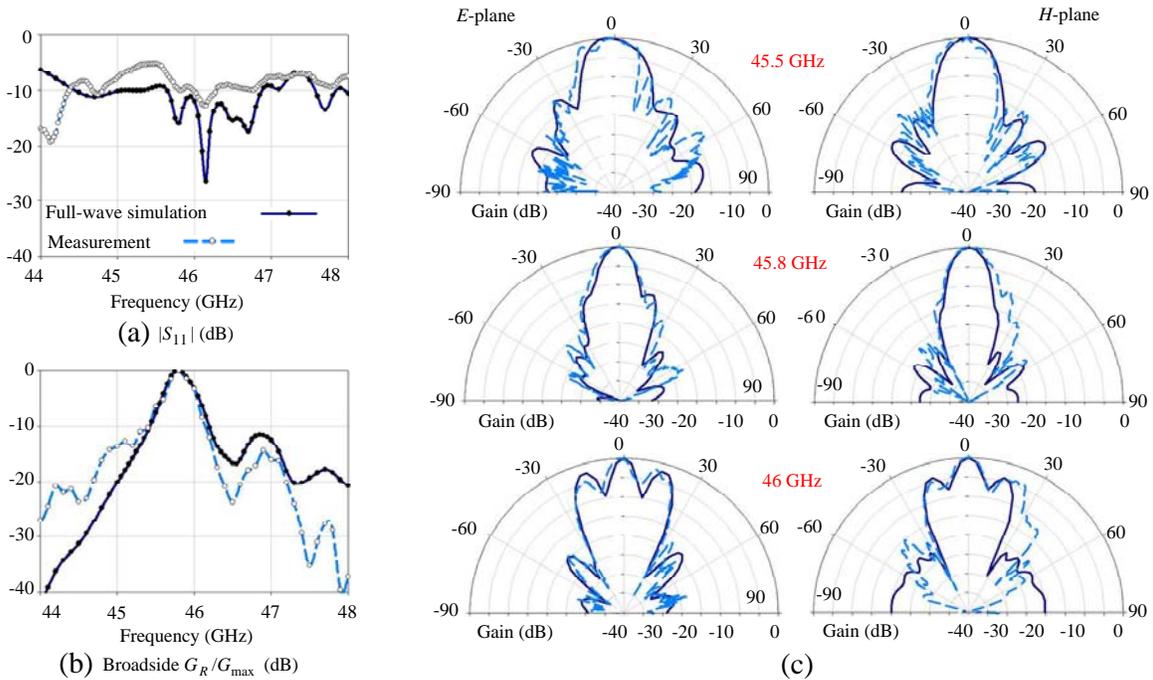
Figure 8. (a) The reflection coefficient, (b) the normalized realized broadside gain of the HG antenna, (c) the normalized gain patterns in both E- and H-planes (a compariosn between the full-wave simulation and measurement results).

Table 2. Summary of simulated and measured results.

FSS	TL			Full-wave			Measurement		
	f_G (GHz)	G_A (dB)	G_ABW (GHz)	f_G (GHz)	G_R (dB)	G_RBW (GHz)	f_G (GHz)	G_R (dB)	G_R BW (GHz)
1	42.9	12	1.11	43.4	9.30	0.70	43.3	11.3	1.35
2	44.2	15.2	0.58	44.6	14.9	0.38	44.6	14	0.45
3	45.6	19.6	0.21	45.8	19.6	0.34	45.8	17	0.3

the E-plane. It can be observed that for HG FPC antennas, the radiation patterns mainly depend on the cavity and FSS rather than the feeding structure.

The cross-polarized patterns of the fabricated antennas are also measured in both E and H-planes; however, since the maximum measured cross-pol gain of the antennas is approximately 35 dB below one of the co-pol, the cross-pol patterns are not shown here for the sake of brevity. The full-wave radiation efficiencies of the designed FPC antennas, accounting also of the losses in the CPW, evaluated at the peak gain frequency of each antenna, are 87%, 85% and 82% for LG, MG and HG antennas, respectively. Table 2 shows a summary of three sets of results: those obtained applying TL theory, those based on full-wave simulations, and those measured. There are some slight differences between the measured gain values and simulated ones, which can be explained based on three facts:

1) The designed antennas (based on TL) are assumed to be infinitely extended along the xy-plane and fed by an elementary magnetic dipole, whereas the full-wave simulated and the fabricated antennas have a finite size and they are also excited by the slot-dipole, fed through a CPW line at the edge of the antenna.

2) The theoretical gain values (based on TL) do not include the mismatch effect at the input port and the losses due the CPW line feeding the slot-dipole.

3) The measurements are carried-out on the uncut wafer whereas the full-wave simulations are done for each single antenna.

Moreover, looking at the measurement plots, Figures 6 to 8, following observations can be summarized as:

1) The radiation patterns in the E-plane of the antenna are asymmetric. This can be explained due to placing of the feeding line in this plane. However, this asymmetry becomes negligible as the gain of the antenna increases.

2) The E-plane and H-plane radiation patterns become more similar as the gain of the antenna increases.

3) As expected, the gain bandwidth of the decreases as the maximum gain of the antenna increases (i.e., by using more reflective FSSs).

4) Considering the differences between the simulated and fabricated structures, for highly-directive FPCs, there is a better match between the measured and simulated gain plots at around f_G, as shown in Figures 7(b) and 8(b).

6. CONCLUSION

It was shown how a single-layer FPC antenna can be considered as a reliable, easy-to-design, and low-cost solution to achieve highly-efficient directive radiation especially at MMWs. The analytical design values, using the TL model of the antenna and backed by LW explanation of each cavity, are verified using full-wave simulations and then measurement results. This type of antenna can be integrated with other printed and/or lumped passive and active components on the same board and therefore proposes a promising solution for MMW technological standpoint. The design is scalable to higher frequencies since it is based on a single-layer dielectric. The power/gain bandwidth is not very wide and can be improved by using a lower permittivity substrate or by resorting to more complicated FSSs as it will be discussed in future work.

REFERENCES

1. Oleski, P. J., "GBS/Milstar airborne RX and TX antenna," *Proc. Military Communications Conf.*, Vol. 2, 599–603, 2000.

2. Biglarbegian, B., M. Fakharzadeh, M. R. Nezhad-Ahmadi, et al., "Optimized patch array antenna for 60 GHz wireless applications," *IEEE Intl. Symp. Antennas Propag.*, 1–4, Toronto, Ontario, Canada, Jul. 2010.

3. Tseng, C.-H., C.-J. Chen, and T.-H. Chu, "A low-cost 60-GHz switched-beam patch antenna array with Butler matrix network," *IEEE Antennas Wirel. Propag. Letters*, Vol. 7, 432–435, 2008.

4. Zhao, T. X., D. R. Jackson, J. T. Williams, et al., "General formulas for 2-D leaky-wave antennas," *IEEE Trans. Antennas Propag.*, Vol. 53, No. 11, 3525–3533, 2005.

5. Lovat, G., P. Burghignoli, and D. R. Jackson, "Fundamental properties and optimization of broadside radiation from uniform leaky-wave antennas," *IEEE Trans. Antennas Propag.*, Vol. 54, No. 5, 1442–1452, 2006.

6. Hosseini, S. A., F. Capolino, F. De Flaviis, et al., "Improved method to estimate the 3 dB power bandwidth of a Fabry-Pérot cavity antenna covered by a thin frequency selective surface," *IEEE Intl. Symp. Antennas Propag.*, 1–4, Spokane, WA, Jul. 2011.

7. Lovat, G., P. Burghignoli, F. Capolino, et al., "Highly-directive planar leaky-wave antennas: A comparison between metamaterial-based and conventional designs," *Proc. Europ. Microw. Assoc.*, Vol. 2, 12–21, 2006.

8. Ostner, H., E. Schmidhammer, J. Detlefsen, et al., "Radiation from dielectric leaky-wave antennas with circular and rectangular apertures," *Electromagnetics*, Vol. 17, 505–535, 1997.

9. Sauleau, R., P. Coquet, and T. Matsui, "Low-profile directive quasi-planar antennas based on millimeter wave Fabry-Perot cavities," *Proc. Microw. Antennas Propag.*, Vol. 150, 274–278, 2003.

10. Lee, Y., X. Lu,, Y. Hao, et al., "Low-profile directive millimeter-wave antennas using free-formed three-dimensional (3-D) electromagnetic bandgap structures," *IEEE Trans. Antennas Propag.*, Vol. 57, No. 10, 2893–2903, 2009.

11. Franson, S. J. and R. W. Ziolkowski, "Gigabit per second data transfer in high-gain metamaterial structures at 60 GHz," *IEEE Trans. Antennas Propag.*, Vol. 57, No. 10, 2913–2925, 2009.

12. Hosseini, S. A., F. Capolino, and F. De Flaviis, "A 44 GHz single-feed Fabry-Pérot cavity antenna designed and fabricated on Quartz," *IEEE Intl. Symp. Antennas Propag.*, 1–4, Spokane, WA, Jul. 2011.

13. Hosseini, S. A., F. De Flaviis, and F. Capolino, "A highly directive single-feed Fabry-Perot cavity antenna for 60 GHz technology," *IEEE Intl. Symp. Antennas Propag.*, 1–2, Chicago, IL, Jul. 2012.

14. Burghignoli, P., G. Lovat, F. Capolino, et al., "Directive leaky-wave radiation from a dipole source in a wire-medium slab," *IEEE Trans. Antennas Propag.*, Vol. 56, 1329–1339, 2008.

15. Chemglass Scientific Apparatus, www.chemglass.com.

16. Gardelli, R., M. Albani, and F. Capolino, "Array thinning by using antennas in a Fabry-Perot cavity for gain enhancement," *IEEE Trans. Antennas Propag.*, Vol. 54, No. 7, 1979–1990, 2006.

17. Kelly, J., G. Passalacqua, A. P. Feresidis, et al., "Simulations and measurements of dual-band 2D periodic leaky wave antenna," *Loughborough Antennas and Propaga. Conf.*, 293–296, 2007.

18. Ronciére, O., B. A. Arcos, R. Sauleau, et al., "Radiation performance of purely metallic waveguide-fed compact Fabry-Perot antennas for space applications," *Microw. Opt. Technol. Lett.*, Vol. 49, 2216–2221, 2009.